First published November 19, 2004; doi:10.1152/japplphysiol.00925.2004.

HIGHLIGHTED TOPIC | *Biomechanics and Mechanotransduction in Cells and Tissues*

Thrombin and histamine induce stiffening of alveolar epithelial cells

Xavier Trepat, Mireia Grabulosa, Lara Buscemi, Fèlix Rico, Ramon Farré, and Daniel Navajas

Unitat de Biofísica i Bioenginyeria, Facultat de Medicina, Universitat de Barcelona-Institut d'Investigacions Biomèdiques August Pi i Sunyer, Barcelona, Spain

Submitted 26 August 2004; accepted in final form 11 November 2004

Trepat, Xavier, Mireia Grabulosa, Lara Buscemi, Fèlix Rico, Ramon Farré, and Daniel Navajas. Thrombin and histamine induce stiffening of alveolar epithelial cells. *J Appl Physiol* 98: 1567–1574, 2005. First published November 19, 2004; doi:10.1152/japplphysiol.00925.2004.—The mechanical properties of alveolar epithelial cells play a central role in maintaining the physical integrity of the alveolar epithelium. We studied the viscoelastic properties of alveolar epithelial cells (A549) in response to thrombin and histamine with optical magnetic twisting cytometry. Ferrimagnetic beads coated with Arg-Gly-Asp (RGD)-peptide or acetylated low-density lipoprotein were bound to cell surface receptors and subsequently twisted in an oscillatory magnetic field (0.1–100 Hz). The cell storage (G′) and loss (G″) moduli were computed from twisting torque and bead displacement. In measurements with RGD-coated beads, thrombin (0.5 U/ml) induced a rapid and sustained threefold increase in G′ and G″ at ~100 s after challenge. Histamine (100 μM) induced a rapid but transient twofold increase in G′ and G″ with maximum values 60 s after challenge. Posttreatment with cytochalasin D abolished thrombin-induced cell stiffening. G′ increased with frequency following a power law with exponent 0.214. G″ increased proportionally to G′ up to 10 Hz but showed a steeper rise at higher frequencies. Thrombin caused a fall in the power-law exponent (0.164). In measurements with acetylated low-density lipoprotein-coated beads, minor changes (<20%) were observed in G′ and G″ after the addition of thrombin and histamine. F-actin staining revealed that thrombin and histamine induced a profound reorganization of the actin cytoskeleton at the cell periphery and formation of actin bundles. In the mechanically dynamic environment of the lung, cell stiffening induced by thrombin and histamine increases centripetal tension, which could contribute to alveolar barrier dysfunction.

cell mechanics; cell rheology; cytoskeleton mechanics; magnetic twisting cytometry; cytoskeleton reorganization

DISRUPTION OF THE alveolar-capillary barrier is a central feature of acute lung injury (34). The physical integrity of this semipermeable barrier is determined by a dynamic balance between adhesive forces that tether cells to each other and to the extracellular matrix and centripetal forces arising from cytoskeletal tension (8). Given that the alveolar-capillary barrier is subjected to considerable stretching during breathing and mechanical ventilation (30), the cell mechanical properties play a crucial role in regulating this force balance. Cell mechanics can be altered by inflammatory mediators present in the extracellular medium of injured lungs, potentially compromising the alveolar wall integrity. Therefore, a better understanding of the mechanisms that regulate the integrity of the alveolar-capillary barrier in injured lungs requires knowledge of the cell mechanical properties in response to these inflammatory mediators.

Thrombin and histamine have been shown to be implicated in the regulation of the permeability of the pulmonary endothelium (8, 17). In vitro, thrombin and histamine induce gap formation in cultured endothelial monolayers as well as increased intracellular calcium, myosin light chain (MLC) phosphorylation, formation of stress fibers, cytoskeletal remodeling, and modulation of cell-cell and cell-matrix adhesions (12, 21, 22, 25, 32). Moreover, stimulation with thrombin increases endothelial cell stiffness and isometric tension of cell monolayers (3, 21). Although the response of the endothelial side of the alveolar-capillary barrier to thrombin and histamine has been extensively investigated, little is known about the effect of these agents on the regulation of the epithelial barrier integrity and, more specifically, on the mechanical properties of alveolar epithelial cells. Thrombin and histamine can be present in the extracellular medium of alveolar epithelial cells after damaging insults of the endothelial barrier, and, consequently, they can play a relevant role in the physiopathology of the alveolar-capillary barrier (6).

The aim of this work was to study the effect of thrombin and histamine on the mechanical properties of alveolar epithelial cells. Optical magnetic twisting cytometry (OMTC) (11) was used to measure the cell complex elastic modulus (G*) of A549 human alveolar epithelial cells in culture. In this technique, ferrimagnetic beads are bound to the cell surface and subsequently twisted in an oscillatory magnetic field. The cell elastic and frictional properties are derived from the ratio between the applied torque and the resulting bead displacement. Cell viscoelasticity data were analyzed on the basis of the soft glassy cell model, which provides a framework for predicting the cell response to different stimulations (9, 29). Changes induced by thrombin and histamine in the actin cytoskeleton were analyzed concurrently with mechanical measurements.

MATERIALS AND METHODS

Cell culture. Human alveolar epithelial cells A549, culture line CCL-185 (ATCC, Manassas, VA) were used. Cells were cultured in HEPES-buffered RPMI 1640 (GIBCO, Gaithersburg, MD) with 10% inactivated fetal calf serum (Biological Industries, Kibbutz Beit Haemek, Israel), 1 mM L-glutamine, 100 U/ml penicillin, 100 mg/ml streptomycin (GIBCO), and 2 μg/ml amphotericin B (Bristol-Myers Squibb, New Brunswick, NJ).

Address for reprint requests and other correspondence: D. Navajas, Unitat de Biofisica i Bioenginyeria, Facultat de Medicina, Casanova 143, 08036-Barcelona, Spain (E-mail: dnavajas@ub.edu).

The costs of publication of this article were defrayed in part by the payment of page charges. The article must therefore be hereby marked "*advertisement*" in accordance with 18 U.S.C. Section 1734 solely to indicate this fact.

Cell-bead preparation. For OMTC experiments, cells were harvested with a brief exposure to trypsin EDTA (Sigma Chemical, St. Louis, MO) and plated (3×10^4 cells/well) on plastic wells (6.4 mm, 96-wells, Costar, Cambridge, MA) that were coated overnight with 100 μl of 5 μg/ml rat tail collagen I at 4°C. Between 20 and 24 h after plating, 10 μg of coated ferrimagnetic beads (Fe_3O_4) of 4.5-μm diameter with magnetic moment 8.9×10^{-13} Am^2 (J. J. Fredberg, Harvard School of Public Health, Boston, MA) were suspended in HEPES-buffered RPMI 1640 with 1% BSA (Sigma Chemical) and added to an individual well. After 20 min incubation at 37°C and 5% CO_2 to allow for binding of the beads to the cell surface, the well was washed with HEPES-buffered RPMI 1640 to remove unbound beads. The sample was then mounted on the experimental setup to perform the OMTC protocols (see *Measurements*).

Unless otherwise specified, the beads were coated with a synthetic RGD (Arg-Gly-Asp)-containing peptide (Peptite 2000, Integra Life Sciences, San Diego, CA) at 50 μg of peptide/mg bead in 1 ml of carbonate buffer (pH 9.4). In a series of experiments, the beads were coated with acetylated low-density lipoprotein (acLDL; Biomedical Technologies, Stoughton, MA) at a density of 50 μg of protein/mg bead in 1 ml of PBS.

OMTC. Cell mechanical properties were measured with OMTC (11). This technique is based on twisting ligand-coated ferrimagnetic microbeads bound to membrane receptors and on measuring the resulting bead displacement with videomicroscopy. Two pairs of orthogonal coaxial coils (magnetizing and twisting pairs) were mounted on an inverted optical microscope (Axiovert S100 Zeiss, Gottingen, Germany) placed on a vibration isolation table (Isostation, Newport, Irvine, CA). The beads were permanently magnetized in the horizontal direction with a brief (10 ms) and large (150 mT) pulse of magnetic field produced by discharging a capacitor (1 mF, 300 V) into the magnetizing pair. Subsequently, the beads were twisted by an oscillatory magnetic field generated by the twisting pair in the vertical direction. The twisting coils were fed with a sinusoidal current of up to 3-A amplitude generated by a computer-controlled current source.

Videomicroscopy was performed with a progressive-scan black and white charge-coupled device camera (CV-M10 BX, JAI, Glostrup, Denmark) controlled with an external trigger. The field of view after magnification (×10) was 640 μm × 480 μm. The analog video signal was digitized and transferred to the personal computer memory by an 8-bit-resolution frame grabber (PC Eye4, Eltec, Mainz, Germany). Heterodyne acquisition was used at twisting frequencies >10 Hz (10). Both the current fed to the coils and the camera trigger were controlled with an analog-digital/digital-analog peripheral component interconnect board (PCI-MIO-16XE-10, National Instruments, Austin, TX) driven by LabVIEW software (National Instruments).

F-actin staining. A549 cells were plated on 10-mm-diameter coverslips (Knittel Glässer, Braunschweig, Germany) 24 h before experiments (~15,000 cells/coverslip). After each staining protocol (see *Measurements*), cells were washed twice with PBS and fixed in a 3.7% formaldehyde-PBS solution for 10 min at room temperature. After two additional washes with PBS, cells were permeabilized with a solution of 0.1% Triton X-100 in PBS for 3–5 min and again washed with PBS. To localize F-actin, cells were then stained with 0.15 μM phalloidin-tetramethylrhodamine isothiocyanate (Sigma Chemical) in PBS with 1% BSA for 20 min. After being washed twice with PBS, the coverslips were finally mounted on a slide with a mounting medium (Mowiol; Calbiochem, La Jolla, CA). Imaging was performed with a confocal laser scanning microscope (TCS-NT; Leica Microsystems, Heidelberg, Germany) at ×63 magnification.

Measurements. We first investigated the time course of the cell viscoelastic response to thrombin and histamine. The beads were magnetized and subsequently twisted in an oscillatory (0.1 Hz) magnetic field of 3-mT amplitude. After 50 s of baseline recording, thrombin (final concentration 0.5 U/ml), histamine (final concentration 100 μM), or culture medium (control) was added to the well, and data were recorded for 3 additional min. Measurements were carried out in $n = 16$ wells for each treatment.

To assess whether the measurement of the cell viscoelastic response to thrombin and histamine depended on the type of bead anchorage to the cell surface, we used acLDL-coated beads. Unlike RGD-coated beads, which bind tightly to the cell cytoskeleton, acLDL-coated beads bind to low-density lipoprotein receptors of the cell membrane that do not form focal adhesions (23, 33). The beads were magnetized and sinusoidally twisted at 0.1 Hz and 3 mT. As in the previous protocol, thrombin, histamine, or culture medium (control) was added to the wells after 50 s of baseline recording ($n = 9$ wells for each treatment), and data were recorded for 3 additional min.

We next studied the role of the actin cytoskeleton in the cell mechanical response to thrombin. Thrombin (0.5 U/ml) was added to the well, and the beads were magnetized and twisted 5 min later (3 mT, 0.1 Hz). After 50 s recording, cytochalasin D (2 μM) or medium (control) was added to the well and the beads were twisted for 3 additional min ($n = 4$ wells).

To better characterize the cell mechanical response to thrombin, we studied the changes induced by this inflammatory mediator in the frequency dependence of cell viscoelasticity. The beads were magnetized and twisted for 10 cycles (10 frames/cycle) at 0.1, 1, 11, and 101 Hz in random order. Measurements were performed under baseline conditions and 5 min after addition of thrombin (0.5 U/ml) to the well ($n = 8$ wells).

To study the changes induced in the organization of the actin cytoskeleton, F-actin was stained after treating the cells with thrombin (0.5 U/ml), histamine (100 μM), or culture medium (control). Fluorescence images were obtained 1 and 5 min after drug addition.

Data processing. OMTC image analysis was performed with a multiple particle tracking application detailed elsewhere (28). Briefly, the first image of each videomicroscopy recording was thresholded and analyzed to identify the beads according to a set of geometrical parameters (bead size and shape, minimum distance between beads). Then the position of each bead was computed in the subsequent images with nanometer resolution using a centroid algorithm. A moving average filter with a time window of one oscillation period was applied to the recording. Beads with an axis of motion displaced >30° with the direction of magnetization were discarded for the analysis (26). The rest of the beads were considered valid for further data processing.

For viscoelasticity computation we defined the specific torque as the torque per unit bead volume:

$$T = mB/V \quad (1)$$

where V is the bead volume, m is the bead magnetic moment, and B is the applied magnetic field (11). The cell complex elastic modulus $G^*(\omega)$ was computed from the Fourier transforms of the specific torque $[T^*(\omega)]$ and of the resulting bead displacement $[d^*(\omega)]$:

$$G^*(\omega) = G'(\omega) + jG''(\omega) = \frac{T^*(\omega)}{d^*(\omega)} \quad (2)$$

where we define $G'(\omega)$ as a storage modulus and $G''(\omega)$ as a loss modulus, ω is the radian frequency ($\omega = 2\pi f$, f is frequency), and j is the imaginary unit defined as $j^2 = -1$ (* indicates complex number).

For time course experiments, $G'(\omega)$ and $G''(\omega)$ were computed for each oscillatory cycle recorded; i.e., we obtained one independent value of $G'(\omega)$ and $G''(\omega)$ every 10 s (f = 0.1 Hz). In these experiments, changes induced by thrombin or culture medium (control) in G' and G'' were evaluated between the average values of the first and last 30 s recorded. Changes induced by histamine were evaluated between the average values of the first 30 s recorded and of those of the time interval 90–120 s of the recording. The time course response of G' and G'' to treatment with cytochalasin D was evaluated as the mean of each minute recorded. For frequency dependence experi-

ments, a single value of $G'(\omega)$ and $G''(\omega)$ was computed from the 10 cycles of recording of each frequency probed.

Modeling. The frequency dependence data $G^*(\omega)$ were fitted with the power-law structural damping equation with the addition of a Newtonian viscous term (9, 13, 24):

$$G^*(\omega) = G_0\left(\frac{\omega}{\omega_0}\right)^{x-1}(1 + j\eta)\Gamma(2 - x)\cos\left[\frac{\pi(x - 1)}{2}\right] + j\omega\mu \quad (3)$$

with

$$\eta = \tan\left[\frac{\pi(x - 1)}{2}\right] \quad (4)$$

where η is the hysteresivity or structural damping coefficient, μ is a Newtonian viscous coefficient, and Γ denotes the gamma function. G_0 and ω_0 are scaling factors for stiffness and frequency, respectively. In this model, $G'(\omega)$ increases with frequency following a power law with exponent $x - 1$. At low frequencies, the Newtonian viscous term $\omega\mu$ can be neglected, and the frequency dependence of $G''(\omega)$ parallels that of $G'(\omega)$ with a ratio $G''(\omega)/G'(\omega) \approx \eta$. At high frequencies, the viscous term comes into play and $G''(\omega)$ approaches the linear dependence of a Newtonian fluid. Excluding the Newtonian viscous term, *Eqs. 3* and *4* comprise the soft glassy cell model introduced by Fabry and coworkers (9). This model assumes that G_0, ω_0, and μ are roughly constant within a given cell type. Accordingly, for the model fitting, G_0, ω_0, and μ were constrained to be constant among treatments and only x was allowed to vary. Therefore, two values of x were obtained from the fitting, corresponding to untreated cells and to cells treated with thrombin, but a single value of G_0, ω_0 and μ was computed. Fitting was carried out by nonlinear regression analysis (MATLAB, The MathWorks, Natick, MA).

Statistics. Because data from OMTC measurements follow a log-normal distribution (9), G' and G'' were computed for each well as the median of all the valid beads (30–60 beads per well) in the field of view of the camera. Unless stated to the contrary, data are reported as means ± SE of the n wells probed in each study. Differences between results obtained with different experimental conditions were analyzed by a paired or unpaired Student's t-test, as appropriate. Statistical significance was assumed at $P < 0.05$.

RESULTS

Measurement of the cell complex elastic modulus revealed that thrombin induced a fast approximately threefold increase in G' and in G'' (Fig. 1) ($P < 0.001$). Baseline values were $G' = 418 \pm 38$ Pa/μm and $G'' = 149 \pm 15$ Pa/μm. A plateau was reached ~100 s after thrombin addition with values of $G' = 1{,}146 \pm 61$ Pa/μm and $G'' = 435 \pm 31$ Pa/μm. Histamine induced a fast but transient approximately twofold increase in G' and in G'' ($P < 0.001$) with maximum values attained ~60 s after drug addition (Fig. 2). Peak values of G' and G'' were 731 ± 80 and 246 ± 28 Pa/μm, respectively. Baseline values of G' and G'' were not fully recovered 3 min after histamine addition ($P < 0.01$). No significant changes were observed when culture medium (control) was added to the wells (Figs. 1 and 2).

When acLDL-coated beads were used to probe cell viscoelasticity, baseline values of G' (27.9 Pa/μm ± 1.6 Pa/μm) and G'' (6.9 Pa/μm ± 0.7 Pa/μm) were ~15-fold lower than those obtained with RGD-coated beads. The cell response to thrombin and histamine was considerably attenuated when measured with acLDL-coated beads (Fig. 3). Thrombin induced a small but significant increase in G' (20%, $P < 0.05$) but not in G''. No significant changes were observed in G^* after addition of histamine or culture medium.

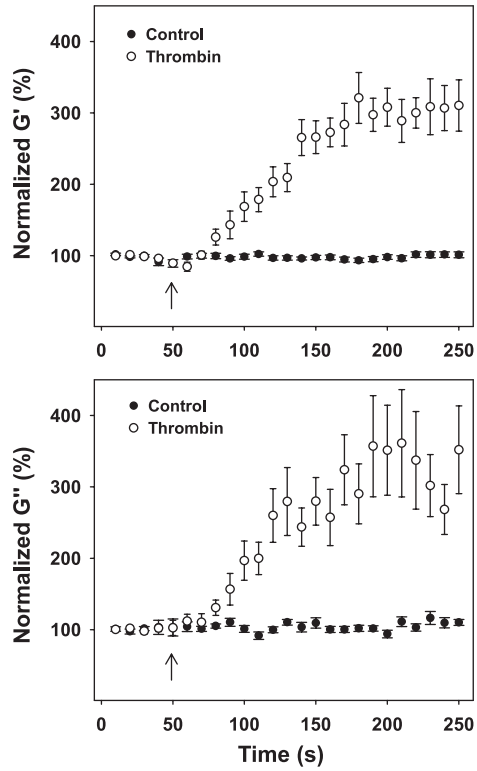

Fig. 1. Cell storage modulus (G'; *top*) and loss modulus (G''; *bottom*) in response to thrombin (○) and to culture medium (●). G' and G'' were normalized to the first 30 s of baseline recording. Arrows indicate addition of thrombin (final concentration 0.5 U/ml; $n = 16$ wells) or medium ($n = 16$ wells). Data are plotted as means ± SE.

Thrombin-induced cell stiffening was progressively abolished by cytochalasin D, as shown in Fig. 4. After 3 min of cytochalasin D addition, G' and G'' dropped to 66% ($P < 0.05$) and 60% ($P < 0.05$) of the plateau values obtained after thrombin treatment, respectively. Addition of culture medium instead of cytochalasin D did not induce significant changes in G' and in G'' ($P > 0.6$).

In untreated cells, G' increased with frequency following a power law with a weak exponent (Fig. 5, *top*). At low frequencies, G'' was approximately threefold lower than G' and increased following a power law with the same exponent (Fig. 5, *bottom*). However, G'' exhibited a steeper frequency dependence at high frequencies approaching the behavior of a Newtonian fluid. This behavior was not only followed by the average cell population but also by all individual cells as reflected by the mean correlation coefficient obtained from the fitting of the structural damping law to all the individual beads ($r^2 = 0.91 \pm 0.11$, mean + SD, $n = 227$ beads). Thrombin induced a rise in both G' and G'' at all probed frequencies. The fit of the structural damping equation (*Eqs. 3* and *4*) to the whole data set (baseline and thrombin treatment) yielded a high correlation coefficient ($r^2 > 0.971$). Increases in cell stiffness were coupled to decreases in the slope of the log-log plots displayed in Fig. 5. Values for the power-law exponent ($x - 1$) obtained from the fit were 0.214 for untreated cells and 0.164 for thrombin-treated cells. The Newtonian viscosity coefficient was $\mu = 2.8$ Pa·s/μm, and the scaling parameters for stiffness and frequency were $G_0 = 96$ kPa/μm and $\omega_0 = 1.8 \times 10^{10}$ rad/s, respectively.

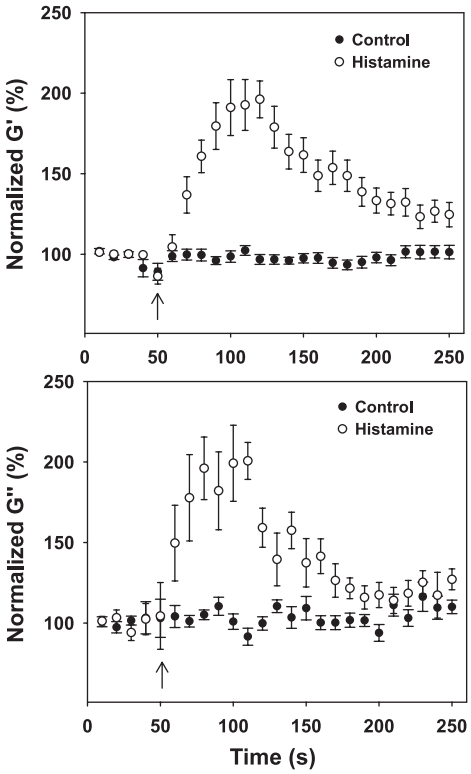

Fig. 2. G′ (*top*) and G″ (*bottom*) in response to histamine (○) and to culture medium (●). G′ and G″ were normalized to the first 30 s of baseline recording. Arrow indicates addition of histamine (final concentration 100 μM; $n = 16$ wells) or medium ($n = 16$ wells). Data are plotted as means ± SE.

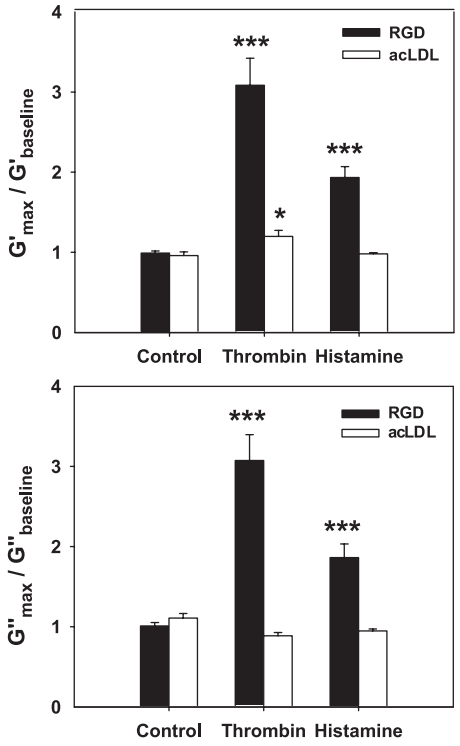

Fig. 3. Changes induced by thrombin and histamine in G′ (*top*) and in G″ (*bottom*) when probed with Arg-Gly-Asp (RGD)-coated beads (solid bars, $n = 16$) and with acetylated low-density lipoprotein (acLDL)-coated beads (open bars, $n = 9$). G′ and G″ were normalized to the first 30 s of baseline recording. Maximum values of G′ and G″ in response to thrombin and control were computed as the average values of the n wells during the last 30 s of recording. Maximum values of G′ and G″ in response to histamine were computed as the average of the recording in the time interval 90–120 s. Data are plotted as means ± SE (***$P < 0.001$; *$P < 0.05$).

F-actin staining revealed a rapid rearrangement of the actin cytoskeleton in response to thrombin and histamine as illustrated in Fig. 6. One minute after thrombin addition, cells exhibited a circumferential organization of F-actin in thick filaments at the cell periphery. This reorganization was more marked 5 min after challenge. Histamine also induced F-actin rearrangement and formation of actin bundles predominantly at the cell periphery at 1 min after agonist addition. Peripheral formation of actin bundles increased 5 min after challenge.

DISCUSSION

We measured the mechanical response of alveolar epithelial cells to thrombin and histamine. Thrombin induced a fast and sustained threefold increase in G′ and G″, and histamine mediated a transient twofold increase in G′ and G″. When cell viscoelasticity was probed with acLDL-coated beads, changes induced by thrombin and histamine in G′ and G″ were substantially smaller than those observed with RGD-coated beads. Cytochalasin D abolished thrombin-induced cell stiffening. The frequency dependence of the cell complex elastic modulus in untreated cells and in cells treated with thrombin conformed to the structural damping power law with the addition of a Newtonian viscous term. Changes in cell mechanics were paralleled by a rapid reorganization of the actin cytoskeleton.

As with other techniques based on microbeads (4, 5), cell mechanical measurements with OMTC require a number of assumptions. In particular, obtaining accurate values of cell viscoelastic properties demands a detailed knowledge of cell-bead geometry. Mijailovich and coworkers (20) proposed a model to estimate the cell shear modulus provided that cell height and percentage of bead embedding were known. Using finite element analysis, these authors reported that the complex shear modulus (G_s^*) can be computed from twisting torque T* and bead displacement d* as $G_s^* = \alpha G^*$, where $G^* = T^*/d^*$ is the apparent complex elastic modulus as we measured in this study (*Eq. 2*) and α is a geometrical factor accounting for cell-bead geometry. In earlier measurements with OMTC, Fabry and coworkers (9) assumed a cell height of 5 μm and a percentage of embedded bead diameter of 10% resulting in

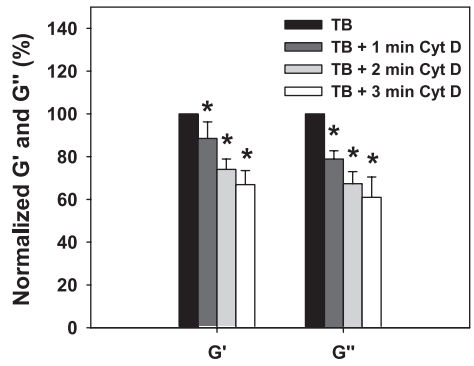

Fig. 4. Effect of adding cytochalasin D (Cyt D; 2 μM) on G′ and G″ of cells pretreated with thrombin (TB; 0.5 U/ml) for 5 min ($n = 4$ wells). Data are plotted as means ± SE (*$P < 0.05$).

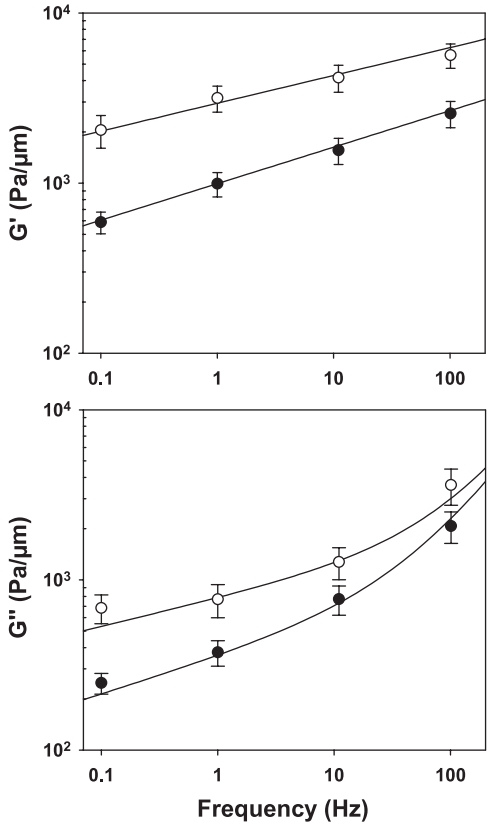

Fig. 5. Frequency dependence of G′ (*top*) and G″ (*bottom*) under baseline conditions (●) and 5 min after thrombin addition (○). Data are plotted as means ± SE. Solid lines are the fit of the structural damping equation (*Eqs. 3* and *4*).

$\alpha = 6.8$ μm. However, a study with confocal microscopy reported that the percentage of RGD-coated bead embedment in alveolar epithelial cells (A549) was highly heterogeneous and ranged from 10 to 45% with a mean value of ~30% (16). According to the analysis of Mijailovich and coworkers (20), this average value of bead embedding would lead to $\alpha \approx 0.93$ μm, resulting in $G'_s = 388$ Pa and $G''_s = 138$ Pa for untreated cells (0.1 Hz). These values are in close agreement with data obtained in our laboratory ($G''_s = 438$ Pa and $G''_s = 146$ Pa) on the same cell type using atomic force microscopy (AFM) (1). This accordance indicates that, despite the model assumptions made, OMTC is a reliable technique to quantitatively measure G*.

Another potential weakness of techniques based on microbeads is that remodeling events associated with bead binding can alter structural properties of the cell probed. Therefore, measurements with OMTC might reflect the mechanical properties of focal adhesion contacts rather than intrinsic cell properties. Again, the agreement of the present study with earlier measurements with AFM argues against this. Indeed, the power-law behavior that we found is in strong accordance with that observed in the same cell type over the same frequency band using AFM (1). Alcaraz and coworkers (1) obtained structural damping behavior with a power-law exponent of $x - 1 = 0.22$, close to the baseline value we obtained in the present study (0.214). These findings indicate that comparable qualitative and quantitative mechanical behavior can be obtained with two techniques that fundamentally differ in the probe specificity. Whereas in this study we probed cell mechanical properties by twisting ligand-coated beads bound to cell receptors, measurements with AFM were performed with uncoated sharp tips that indented the cell apical surface down to 1.5 μm (1). Therefore, the observed mechanical behavior is not attributable to the probe, to receptor kinetics, to membrane mechanics, or to the dynamics of focal adhesion contacts that link beads to the cell surface. Instead, the equivalence between observations found with OMTC and AFM suggests that the mechanical behavior we found reflects intrinsic cytoskeletal properties.

To the best of our knowledge these are the first mechanical measurements of the response of alveolar epithelial cells to proinflammatory stimuli. Previously, Bausch and coworkers (3) studied the response of endothelial cells to thrombin by applying strong force pulses (2 nN) on fibronectin-coated magnetic beads bound to the cell surface. The authors found a rapid and transient increase in bead deflection that was attributed to changes in the coupling of integrin receptors to the actin cortex. By contrast, we observed a sustained increase in cell stiffness. These discrepancies could be explained by the difference in cell type, which would indicate differences in the mechanical response of endothelial and epithelial cells to inflammatory agents. The disagreement could also be explained by differences in the methodological approach. Instead of applying strong pulses of magnetic field (2 nN) resulting in large bead deflections (~500 nm) (3), we smoothly twisted the beads with much smaller displacement amplitudes (~150 nm under baseline conditions and ~50 nm after thrombin addition). Therefore, it is quite possible that our measurements did not mechanically alter the linkages between the integrins and the underlying cytoskeleton as suggested by Bausch and coworkers. The mechanical response to histamine has been extensively studied in airway smooth muscle cells (11, 14, 18). Maksym and coworkers (18) showed that histamine mediated rapid cell stiffening followed by a gradual decrease in G′ and G″. Hence, histamine induced comparable stiffening in alveolar epithelial cells and in airway smooth muscle cells, suggesting that similar mechanisms could be involved in the cell mechanical response to this agonist.

G* increased with bead twisting frequency according to a structural damping power law (*Eqs. 3* and *4*). This empirical relationship assumes that frictional stresses within the cell are proportional to elastic stresses when probed at low frequencies and that the coefficient of proportionality is independent of the loading frequency. This behavior is not maintained at high frequencies owing to a marked increase in cell viscosity (9). When cells were treated with thrombin, the structural damping behavior was preserved. Moreover, *Eqs. 3* and *4* accounted for the observed behavior with a single free variable, i.e., the power-law exponent x. A comparable behavior was recently reported in other cell types subjected to a variety of pharmacological stimuli including histamine, dibutyryl adenosine 3′,5′-cyclic monophosphate, and cytochalasin D (10). On the basis of these measurements, Fabry and coworkers hypothesized that living cells belong to the class of soft glassy materials. Soft glassy materials share in common softness, intrinsic disorder, and power-law frequency dependence of G′ and G″ with a weak exponent (27). Moreover, their dynamic properties are mainly determined by the exponent of the power

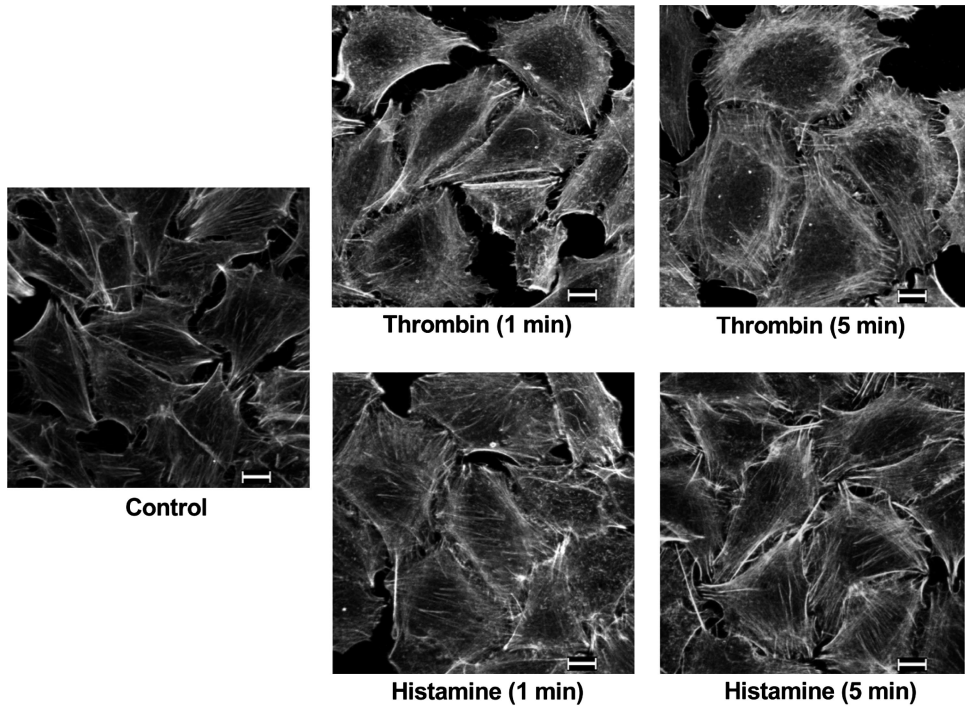

Fig. 6. F-actin staining in control cells (*left*) and in cells treated with thrombin 0.5 U/ml (*top*) and histamine 100 μM (*bottom*) for 1 min (*middle*) and 5 min (*right*). Bar = 10 μm.

law, which is an indicator of internal disorder of the system. Fundamental aspects of the soft glassy cell model, such as identification of the main source of agitation or demonstration that cells exhibit viscoelastic aging phenomena, remain to be elucidated (10). Nonetheless, the empirical framework of the structural damping law provides a powerful tool to predict cell dynamical behavior in response to pharmacological stimulation. Indeed, parameters in *Eqs. 3* and *4*, with the exception of the viscosity term, which can be neglected at physiological frequencies, can be derived from data at one frequency. Therefore, the whole cell frequency dependence as well as the stress-relaxation function can be simply predicted from a single oscillatory measurement (9).

When cell mechanics was probed with acLDL-coated beads, changes in cell stiffness, if any, were found to be considerably lower than those obtained in measurements with RGD-coated beads. Histamine did not induce significant changes in G′ and G″, whereas thrombin induced only a 20% increase in G′. In contrast to RGD-coated beads, acLDL-coated beads bind to nonadhesion receptors of the cell membrane and do not anchor to the actin cytoskeleton through focal adhesions (23, 33). Therefore, the attenuated response measured with acLDL-coated beads indicates that cell stiffening induced by thrombin and histamine arises from the actin cytoskeleton. To provide further evidence of the central role played by the actin cytoskeleton in thrombin-induced cell stiffening we added cytochalasin D after 5 min of treatment with thrombin. Cytochalasin D binds to the barbed end of microfilaments and prevents their elongation, resulting in a rapid depolymerization of F-actin (7). We observed that cytochalasin D progressively reversed the increased stiffness induced by thrombin, which corroborates the determinant role of the actin cytoskeleton in the cell stiffening response.

Different cytoskeleton-dependent mechanisms could account for the increased cell stiffness in response to thrombin and histamine. We observed a marked reorganization of the actin cytoskeleton in response to both inflammatory mediators. Specifically, thrombin induced filament assembly and circumferential rearrangement of F-actin at the cell periphery, in agreement with a recent study by Kawkitinarong and coworkers (15). Histamine also induced rapid formation of F-actin bundles mostly at the cell periphery. Given that we probed cell mechanics with beads bound to the cell surface, the stiffening response to thrombin and histamine could be a reflection of the peripheral reorganization of the actin cytoskeleton. In addition to F-actin reorganization, thrombin and histamine have been reported to increase actin polymerization in other cell types such as endothelial and smooth muscle cells, which could also contribute to cell stiffening (2, 12, 19). The time course of actin polymerization closely matched that of increased cell stiffness in cells challenged with thrombin. However, this was not the case in histamine-treated cells. Whereas cell stiffness increased transiently with a maximum value at 1 min after histamine addition, circumferential formation of F-actin bundles was more marked 5 min after challenge. Hence, although the actin cytoskeleton is required for cell stiffening as shown by acLDL-coated bead measurements, our results suggest that its reorganization is not sufficient to explain the time course of G′ and G″ in response to histamine.

Besides actin polymerization and reorganization, increased cell stiffness could arise from activation of the cell actomyosin apparatus. Thrombin and histamine mediate the activation of the Ca^{2+}/calmodulin-dependent MLC kinase, which phosphorylates the MLC, giving rise to increased filament assembly, actomyosin interaction, motor activity, and force generation (15, 21). The state of phosphorylation of the MLC is also regulated by Rho, which, on activation, can lead to the inhibition of the MLC phosphatase and to the formation of stress fibers (31, 35). Rho has been shown to play a central role in the time course of endothelial cell response to thrombin, but its

role in regulating the cell response to histamine is less clear and might depend on culture conditions (32, 35). Differences in Rho-mediated regulation of the MLC phosphatase by thrombin and histamine could account for the sustained or transient behavior we observed. This different behavior could also be explained by the possibility that thrombin induces higher levels of phosphorylation than histamine, as shown in endothelial cells (21). Further studies should address the relative contribution of actin remodeling and actomyosin contractility to the stiffening response to thrombin and histamine in alveolar epithelial cells.

Pathological features of acute lung injury include damage to the alveolar-capillary barrier with flow of liquid and macromolecules and infiltration of inflammatory cells into the air spaces (34). This increased permeability has been associated with paracellular gap formation in the pulmonary endothelium (8). However, the characteristic traffic of molecules and cells through the alveolar-capillary barrier during lung inflammation also requires disruption of the alveolar epithelium. Thrombin and histamine have been shown to increase permeability of endothelial cells monolayers (21, 32). This increase was fast and sustained for thrombin and fast but transient for histamine. We found a roughly parallel time course in the stiffening of alveolar epithelial cells after application of these inflammatory mediators, which suggests that alveolar epithelial and endothelial cells might regulate alveolar-capillary permeability through integrative mechanisms. The physical integrity of epithelial and endothelial cell monolayers is regulated by a balance between centripetal tensional forces and centrifugal adhesive forces, which tether cells to each other and to their extracellular matrix. Centripetal forces have been attributed to the contraction of the actomyosin machinery (8). However, viscoelastic recoil forces caused by cell stretching during spontaneous or artificial ventilation also contribute to the centripetal force in the cell. The cell stiffening that we found after the application of thrombin or histamine results in increased viscoelastic recoil. This increase in the centripetal forces during cell stretching might not be balanced by the cell-cell and cell-matrix tethering forces, leading to paracellular gap formation and increased permeability of the epithelial monolayer. However, the peripheral cytoskeletal remodeling that we observed in response to thrombin and histamine could strengthen the tethering forces, thereby protecting barrier integrity (15). Further research into the alteration of the force balance in the alveolar epithelium during inflammation will help us to better understand the alveolar-capillary barrier disruption in acute lung injury.

ACKNOWLEDGMENTS

The authors thank Miguel Rodriguez for technical assistance.

GRANTS

This work was supported in part by grants from Ministerio de Ciencia y Tecnologia (SAF 2002-03616 and SAF 2003-01334), Ministerio de Sanidad y Consumo (Red GIRA-G03/063 and Red RESPIRA-C03/11), and National Heart, Lung, and Blood Institute Grant HL-65960.

REFERENCES

1. **Alcaraz J, Buscemi L, Grabulosa M, Trepat X, Fabry B, Farre R, and Navajas D.** Microrheology of human lung epithelial cells measured by atomic force microscopy. *Biophys J* 84: 2071–2079, 2003.
2. **An SS, Laudadio RE, Lai J, Rogers RA, and Fredberg JJ.** Stiffness changes in cultured airway smooth muscle cells. *Am J Physiol Cell Physiol* 283: C792–C801, 2002.
3. **Bausch AR, Hellerer U, Essler M, Aepfelbacher M, and Sackmann E.** Rapid stiffening of integrin receptor-actin linkages in endothelial cells stimulated with thrombin: a magnetic bead microrheology study. *Biophys J* 80: 2649–2657, 2001.
4. **Bausch AR, Ziemann F, Boulbitch AA, Jacobson K, and Sackmann E.** Local measurements of viscoelastic parameters of adherent cell surfaces by magnetic bead microrheometry. *Biophys J* 75: 2038–2049, 1998.
5. **Choquet D, Felsenfeld DP, and Sheetz MP.** Extracellular matrix rigidity causes strengthening of integrin-cytoskeleton linkages. *Cell* 88: 39–48, 1997.
6. **Cocks TM and Moffatt JD.** Protease-activated receptors: sentries for inflammation? *Trends Pharmacol Sci* 21: 103–108, 2000.
7. **Cooper JA.** Effects of cytochalasin and phalloidin on actin. *J Cell Biol* 105: 1473–1478, 1987.
8. **Dudek SM and Garcia JG.** Cytoskeletal regulation of pulmonary vascular permeability. *J Appl Physiol* 91: 1487–1500, 2001.
9. **Fabry B, Maksym GN, Butler JP, Glogauer M, Navajas D, and Fredberg JJ.** Scaling the microrheology of living cells. *Phys Rev Lett* 87: 148102-1–148102-4, 2001.
10. **Fabry B, Maksym GN, Butler JP, Glogauer M, Navajas D, Taback NA, Millet EJ, and Fredberg JJ.** Time scale and other invariants of integrative mechanical behavior in living cells. *Phys Rev E* 68: 041914-1–041914-18, 2003.
11. **Fabry B, Maksym GN, Shore SA, Moore PE, Panettieri RAJ, Butler JP, and Fredberg JJ.** Selected contribution: time course and heterogeneity of contractile responses in cultured human airway smooth muscle cells. *J Appl Physiol* 91: 986–994, 2001.
12. **Goeckeler ZM and Wysolmerski RB.** Myosin light chain kinase-regulated endothelial cell contraction: the relationship between isometric tension, actin polymerization, and myosin phosphorylation. *J Cell Biol* 130: 613–627, 1995.
13. **Hildebrandt J.** Comparison of mathematical models for cat lung and viscoelastic balloon derived by Laplace transform methods from pressure-volume data. *Bull Math Biophys* 31: 651–667, 1969.
14. **Hubmayr RD, Shore SA, Fredberg JJ, Planus E, Panettieri RA Jr, Moller W, Heyder J, and Wang N.** Pharmacological activation changes stiffness of cultured human airway smooth muscle cells. *Am J Physiol Cell Physiol* 271: C1660–C1668, 1996.
15. **Kawkitinarong K, Linz-McGillem L, Birukov KG, and Garcia JG.** Differential regulation of human lung epithelial and endothelial barrier function by thrombin. *Am J Respir Cell Mol Biol* 31: 517–527, 2004.
16. **Laurent VM, Henon S, Planus E, Fodil R, Balland M, Isabey D, and Gallet F.** Assessment of mechanical properties of adherent living cells by bead micromanipulation: comparison of magnetic twisting cytometry vs optical tweezers. *J Biomech Eng* 124: 408–421, 2002.
17. **Lum H and Malik AB.** Mechanisms of increased endothelial permeability. *Can J Physiol Pharmacol* 74: 787–800, 1996.
18. **Maksym GN, Fabry B, Butler JP, Navajas D, Tschumperlin DJ, Laporte JD, and Fredberg JJ.** Mechanical properties of cultured human airway smooth muscle cells from 0.05 to 04 Hz. *J Appl Physiol* 89: 1619–1632, 2000.
19. **Mehta D, Tiruppathi C, Sandoval R, Minshall RD, Holinstat M, and Malik AB.** Modulatory role of focal adhesion kinase in regulating human pulmonary arterial endothelial barrier function. *J Physiol* 539: 779–789, 2002.
20. **Mijailovich SM, Kojic M, Zivkovic M, Fabry B, and Fredberg JJ.** A finite element model of cell deformation during magnetic bead twisting. *J Appl Physiol* 93: 1429–1436, 2002.
21. **Moy AB, Van Engelenhoven J, Bodmer J, Kamath J, Keese C, Giaever I, Shasby S, and Shasby DM.** Histamine and thrombin modulate endothelial focal adhesion through centripetal and centrifugal forces. *J Clin Invest* 97: 1020–1027, 1996.
22. **Murphy JT, Duffy SL, Hybki DL, and Kamm K.** Thrombin-mediated permeability of human microvascular pulmonary endothelial cells is calcium dependent. *J Trauma* 50: 213–222, 2001.
23. **Plopper GE, McNamee HP, Dike LE, Bojanowski K, and Ingber DE.** Convergence of integrin and growth factor receptor signaling pathways within the focal adhesion complex. *Mol Biol Cell* 6: 1349–1365, 1995.
24. **Puig-de-Morales M, Grabulosa M, Alcaraz J, Mullol J, Maksym GN, Fredberg JJ, and Navajas D.** Measurement of cell microrheology by magnetic twisting cytometry with frequency domain demodulation. *J Appl Physiol* 91: 1152–1159, 2001.
25. **Schaphorst KL, Pavalko FM, Patterson CE, and Garcia JG.** Thrombin-mediated focal adhesion plaque reorganization in endothelium: role of protein phosphorylation. *Am J Respir Cell Mol Biol* 17: 443–455, 1997.

26. **Smith PG, Deng L, Fredberg JJ, and Maksym GN.** Mechanical strain increases cell stiffness through cytoskeletal filament reorganization. *Am J Physiol Lung Cell Mol Physiol* 285: L456–L463, 2003.
27. **Sollich P, Lequeux F, Hébraud P, and Cauberghs M.** Rheology of soft glassy materials. *Phys Rev Lett* 78: 2020–2023, 1997.
28. **Trepat X, Grabulosa M, Buscemi L, Rico F, Fabry B, Fredberg JJ, and Farré R.** Oscillatory magnetic tweezers based on ferromagnetic beads and simple coaxial coils. *Rev Sci Instrum* 74: 4012–4020, 2003.
29. **Trepat X, Grabulosa M, Puig F, Maksym GN, Navajas D, and Farre R.** Viscoelasticity of human alveolar epithelial cells subjected to stretch. *Am J Physiol Lung Cell Mol Physiol* 287: L1025–L1034, 2004.
30. **Tschumperlin DJ and Margulies SS.** Alveolar epithelial surface area-volume relationship in isolated rat lungs. *J Appl Physiol* 86: 2026–2033, 1999.
31. **Van Hinsbergh VW and Van Nieuw Amerongen GP.** Intracellular signalling involved in modulating human endothelial barrier function. *J Anat* 200: 549–560, 2002.
32. **Van Nieuw Amerongen GP, Draijer R, Vermeer MA, and Van Hinsbergh VW.** Transient and prolonged increase in endothelial permeability induced by histamine and thrombin: role of protein kinases, calcium, and RhoA. *Circ Res* 83: 1115–1123, 1998.
33. **Wang N, Butler JP, and Ingber DE.** Mechanotransduction across the cell surface and through the cytoskeleton. *Science* 260: 1124–1127, 1993.
34. **Ware LB and Matthay MA.** The acute respiratory distress syndrome. *N Engl J Med* 342: 1334–1349, 2000.
35. **Wojciak-Stothard B and Ridley AJ.** Rho GTPases and the regulation of endothelial permeability. *Vascul Pharmacol* 39: 187–199, 2002.